ENVIRONMENTAL RESEARCH
LETTERS

LETTER • **OPEN ACCESS**

Post-disturbance ice-wedge degradation in Alaskan tundra fire scars using space-for-time substitution remote sensing

To cite this article: T Rettelbach *et al* 2026 *Environ. Res. Lett.* **21** 054010

ENVIRONMENTAL RESEARCH
LETTERS

LETTER

Post-disturbance ice-wedge degradation in Alaskan tundra fire scars using space-for-time substitution remote sensing

T Rettelbach[1,2,3,9,*], **J Bader**[4], **B Groenke**[1,5], **V Helm**[6], **M Langer**[1,7], **J-C Freytag**[3,8] and **G Grosse**[1,2]

[1] Permafrost Research Section, Alfred Wegener Institute, Telegrafenberg A45, 14473 Potsdam, Germany
[2] Institute of Geosciences, University of Potsdam, Karl-Liebknecht-Str. 24-25, 14476 Potsdam, Germany
[3] Einstein Center Digital Future, Wilhelmstr. 67, 10117 Berlin, Germany
[4] Research Group Distributed and Operating Systems, Technische Universität Berlin, Einsteinufer 17, 10587 Berlin, Germany
[5] Department of Complexity Science, Potsdam Institute for Climate Impact Research, Telegrafenberg, 14412 Potsdam, Germany
[6] Glaciology Research Section, Alfred Wegener Institute, Am Alten Hafen 26, 27568 Bremerhaven, Germany
[7] Faculty of Science, Earth and Climate, Vrije Universiteit Amsterdam, De Boelelaan 1085, 1081 HV Amsterdam, The Netherlands
[8] Department of Computer Sciences, Databases and Information Systems, Humboldt-Universität zu Berlin, Unter den Linden 6, 10099 Berlin, Germany
[9] Now at: Department of Space Research and Space Technology, Technical University of Denmark, Elektrovej B327, 2800 Kgs. Lyngby, Denmark.
[*] Author to whom any correspondence should be addressed.

E-mail: stare@dtu.dk

OPEN ACCESS

RECEIVED
22 September 2025

REVISED
12 February 2026

ACCEPTED FOR PUBLICATION
23 February 2026

PUBLISHED
3 March 2026

Keywords: permafrost landscapes, tundra fire, ice-wedge degradation, remote sensing, airborne lidar, graph analysis, Alaska

Supplementary material for this article is available online

Abstract

The severity and frequency of tundra fires in Arctic permafrost landscapes is expected to increase with ongoing climate change. By burning the insulating organic layer of soils, tundra fires impact the soil thermal regime for underlying permafrost and can accelerate thaw in the years following the burn. In this paper, we address the scarcity of long-term studies on post-fire permafrost degradation in ice-wedge landscapes by using a space-for-time substitution analysis spanning a chronosequence (pseudo-time series) of up to 67 years of remote sensing data from Alaskan tundra fire scars. We use computer vision and graph analysis on high-resolution digital elevation models derived from airborne lidar of fire-affected areas in Western Alaska to investigate the effects of tundra fires on the post-fire development of microtopography and surface hydrology in polygonal ice-wedge landscapes. Our analysis indicates a modest overall trend toward recovery of polygonal surface structure over timescales of 70+ years, though considerable variability among fire scars highlights that post-fire trajectories are not uniform.

1. Introduction

Permafrost landscapes throughout Arctic tundra ecosystems face increasing pressures due to climate change-induced phenomena. Recent studies observed an average increase of mean annual permafrost ground temperatures of $0.39 \pm 0.15\,^{\circ}\mathrm{C}$ in the continuous permafrost zone compared to the 2007–2016 average [1], and a reduction in permafrost extent over the past centuries in several Subarctic permafrost regions. This permafrost thaw promotes carbon release into the atmosphere [2, 3], and can result in shifting vegetation patterns [4], changes in hydrological regimes [5], or topographical changes—all with major consequences to permafrost ecosystems. Permafrost thaw can be categorized as either gradual or non-gradual (also 'abrupt') [6]. Gradual thaw unfolds over decades to centuries through the thickening of the active layer, the top layer of soil above permafrost that thaws and refreezes seasonally. Conversely, non-gradual thaw occurs over significantly shorter timescales (days to years), and is often triggered by more sudden ground-ice melt following disturbance. It involves terrain subsidence and erosion, creating landforms such as retrogressive thaw slumps or thermo-erosion gullies, potentially even exposing deep permafrost layers to above-freezing temperatures [6]. However, since

these abrupt changes are connected to disturbances, they are less predictable and thus pose significant challenges for estimating the impacts on the regional environment or on infrastructure and local communities.

One notable disturbance known to trigger abrupt thaw under certain conditions is tundra fire [2, 7, 8]. Several studies have shown that fire frequency and severity are expected to increase with ongoing climate warming, which will promote conditions under which post-fire permafrost thaw occurs [9, 10]. Particularly in ice-rich permafrost landscapes, such as those characterized by ice-wedge polygons, severe tundra fires can have substantial consequences: By burning the insulating vegetation and topmost organic soil layers, these fires directly emit large amounts of carbon [11] but also affect the long-term soil thermal regime by destroying the buffer between the atmosphere and frozen ground below, thus strongly increasing the vulnerability of these already fragile tundra environments to warming. The subsequent degradation of ice-wedge landscapes due to tundra fires not only alters terrain properties but also perpetuates further permafrost degradation, which manifests as ground subsidence [7], increasing surface and ground temperatures as well as an initial thickening of the active layer [8, 12], and shifts in nutrient dynamics [13] and vegetation patterns [14], all with far-reaching consequences for permafrost ecosystem functioning and resilience [15, 16].

Most studies on post-fire ice-wedge degradation have been conducted in the Anaktuvuk River Fire scar in Northslope, Alaska, where one of Alaska's largest and most severe tundra fires burned about 1000 km^2 in summer 2007 [7, 11, 17–20]. These studies shed light on the dynamics of permafrost degradation on short time scales of several years and suggest a positive correlation between the time elapsed since a fire and the extent of landscape degradation. Subsequent work [21] suggests that the ice-wedge polygon degradation in this fire scar has stabilized 15 years post-disturbance. Such pathways of stabilization and even recovery of degrading ice-wedge troughs has previously been theorized by [22] and validated with in-situ observations by [23], who showed that under certain environmental conditions, ice-wedge degradation can decelerate, stabilize, and sometimes revert so that landscapes resemble undisturbed terrain. Stabilization and recovery processes can for example be initiated through the accumulation of peat in the troughs or drainage of the trough ponds [22]. Despite considerable advancements in understanding post-fire permafrost dynamics, it remains unclear whether recovery after ice-wedge degradation is a rare or widespread phenomenon due to a significant gap in long-term decadal-scale observations spanning a larger number of fire scars. Analyzing long remote sensing time series is our best approach to tackle this issue and some prior investigations even used terrain texture and vegetation characteristics in imagery to identify burn scars from fires predating the remote sensing record [24]. Our understanding of the time scales of post-disturbance permafrost thaw, stabilization, and recovery processes stems mostly from few field studies or detailed local-scale remote sensing studies (e.g. [8, 25, 26]). Such data is still sparse but is hugely important for quantifying the effects of fire return intervals, biogeochemical and hydrological impacts, vegetation and ecosystem succession, and overall landscape trajectories in disturbance settings.

Our study aims to address this knowledge gap by employing a space-for-time substitution remote sensing analysis to investigate the long-term effects of tundra fires on landscape microtopography and surface hydrology. By analyzing more than 100 areas of interests (AOIs) within and around fire scars in Western Alaska, USA, we aim to investigate the post-fire pathways of ice-wedge degradation and stabilization in these disturbance settings. Leveraging image segmentation and graph extraction techniques, as outlined by [20], we provide insights into the utility of such methodologies to quantify landscape dynamics on larger spatial scales. We also demonstrate the scalability of our pipeline with the workflow manager Nextflow (see supplementary material B), ensuring reproducibility and portability in preparation for application to the growing archive of high-resolution elevation data such as airborne light detection and ranging (lidar).

2. Study area

Our investigation focuses on fire scars within two distinct ecoregions of Western Alaska: the Noatak River Valley (NRV, figures 1(a) and (b)) and the Central Seward Peninsula (CSP, figures 1(c) and (d)), with a subset in the Buckland River Valley (BRV, figure 1(e)). We refer to the CSP together with the BRV as Seward Peninsula (SP). This classification aligns with previous studies by [16, 27]. According to [28], all selected study sites lie within the discontinuous permafrost zone, with permafrost coverage ranging from 50% to 90%. Analysis of the fire history in both regions reveals more frequent occurrences of tundra fires in the NRV (mean fire interval (MFI) of 13 years), with smaller average areas burned (13.8 km^2), while the SP has encountered larger fires (on average 39.1 km^2), albeit at lower frequency (MFI of 18 years). The fire rotation period (FRP) is at 425 (NRV) and 424 (SP) years and thus almost identical in both ecoregions [16]. In the NRV study area, the landscape is characterized by thermokarst lakes within once-glaciated

Table 1. Environmental and fire regime properties for the Seward Peninsula and Noatak River Valley study regions. Numbers reported refer to specified locations (in brackets), or the larger region. Region definitions vary and can be gathered from the cited references. MAGT: mean annual ground temperature; MAAT: mean annual air temperature; MAP: mean annual precipitation; ALT: active layer thickness; OLT: organic layer thickness; SOC: soil organic carbon; MFI: mean fire interval; FRP: fire rotation period.

	SP	NRV	References
Permafrost extent	Discontinuous/continuous	Discontinuous/continuous	[28]/[31]
MAGT (2000–2016)	$-1.27 \pm 1.97\,^{\circ}$C	$-1.74 \pm 1.97\,^{\circ}$C	[28]
Vegetation types	sedge, lichen, tussock tundra with dwarf shrubs in valley bottoms	shrub-sedge, lichen, and tussock tundra, with tall shrubs and willow and birch thickets along rivers and valley bottoms	[34]
MAAT (1991–2020)	$-2.2\,^{\circ}$C (Nome)	$-4.4\,^{\circ}$C (Kotzebue)	[35]
MAP (1991–2020)	437 mm (Nome)	290 mm (Kotzebue)	[35]
ALT (mean 2001–2015)	75 cm	70 cm	[36]
OLT (unburned, summer mean 2016–2018)	19.27 ± 8.35 cm	14.64 ± 7.60 cm	[27]
SOC (0–0.3 m)	6–13 kg · m^{-3}	9–19 kg · m^{-3}	[37]
Soil moisture (vol. frac.)	0.85 (0–0.05 m), 0.9 (0–1 m)	0.85 (0–0.05 m), 0.9 (0–1 m)	[38]
Fire ecoregion area	47 307 km^2	15 049 km^2	[16]
Total area burned	7171 km^2	2465 km^2	[39]
MFI (1950–2011)	18 years	13 years	[16]
FRP (1950–2011)	424 years	425 years	[16]
Fire years at AOIs	1954, 1971, 1977, 1997, 2002, 2015	1977, 1999, 2004, 2012	[39]

valleys. Conversely, the SP shows rolling tundra landscapes dominated by sedge tussock communities, with shrubs primarily found in valley bottoms of the Kougarok and the Buckland Rivers. Table 1 summarizes the site characteristics.

Within these ecoregions, we conducted airborne lidar surveys covering a wide range of fire scars and within these areas we randomly sampled 500 square plots to investigate the presence, abundance, and morphology of polygonal patterns in detail. As these plot AOI need to be of equal size and shape to allow quantitative comparison of graph metrics [20], we chose a size of 30.25 ha (550 m by 550 m). This size allowed a maximization of the number of AOIs with fairly homogeneous land surface in the available lidar footprints while also covering a minimum potential number of polygon features, which typically have diameters of 10–15 m, in each AOI. As the graph extraction is only stable within landscapes of high-centered polygons, we manually remove any AOIs sampled in low-centered polygonal terrain and any AOIs that were sampled in lakes or rivers. This left us with 106 AOIs overall; 62 in SP, and 44 in NRV. Respectively, three and 11 of these remaining AOIs are 'reference plots' that are located in unburned[10] areas close to the fire scars. Due to the short MFI in both study regions, it was not possible to restrict AOI sampling to areas that have burned only once. Several of the 92 fire-AOIs are located in terrain that has experienced up to four fires since 1954. Previous research has demonstrated that repeated burning in tundra landscapes can alter the vegetation structure and dynamics [29], however, their effect on ice-wedge polygon topography has not been quantified, to the best of our knowledge. A statistical analysis on the relevance of multiple burns towards our results has shown us that the fire frequency does not exert significant influence on the post-fire evolution of the polygonal networks (see supplementary material A).

The soil and environmental characteristics for these two areas are similar throughout and we therefore consider both as belonging to the same ecoregion (see also [16, 30]). For SP, the furthest AOIs are 201 km apart if we consider both subgroups of CSP and BRV; or 38 km apart if we only consider the AOIs in CSP (where the majority of SP AOIs lie, see figure 1(e)), with 72 m elevation difference. In the SP region, the oldest burn happened in 1954. Considering our datasets collected in 2021 (section 3.1.2), this creates a pseudo-time series with fire scars spanning time since burn from five to 67 years. In the NRV region, the furthest AOIs are 74 km apart and the AOI at the highest elevation is located 150 m higher than the one at the lowest. Here, where the oldest fire occurred in 1977, the pseudo-time series spans fire scars with time since burn from nine to 45 years. Information on fire age and location was taken from the ALFD (section 3.1.1). We determined the ground-ice and soil deposit characteristics for our study sites based on [31] (figure 2). The SP AOIs feature deposits with higher ice content and a mostly silty composition. The majority of deposits are

[10] Unburned according to the Alaska Large Fire Database (ALFD) (section 3.1.1).

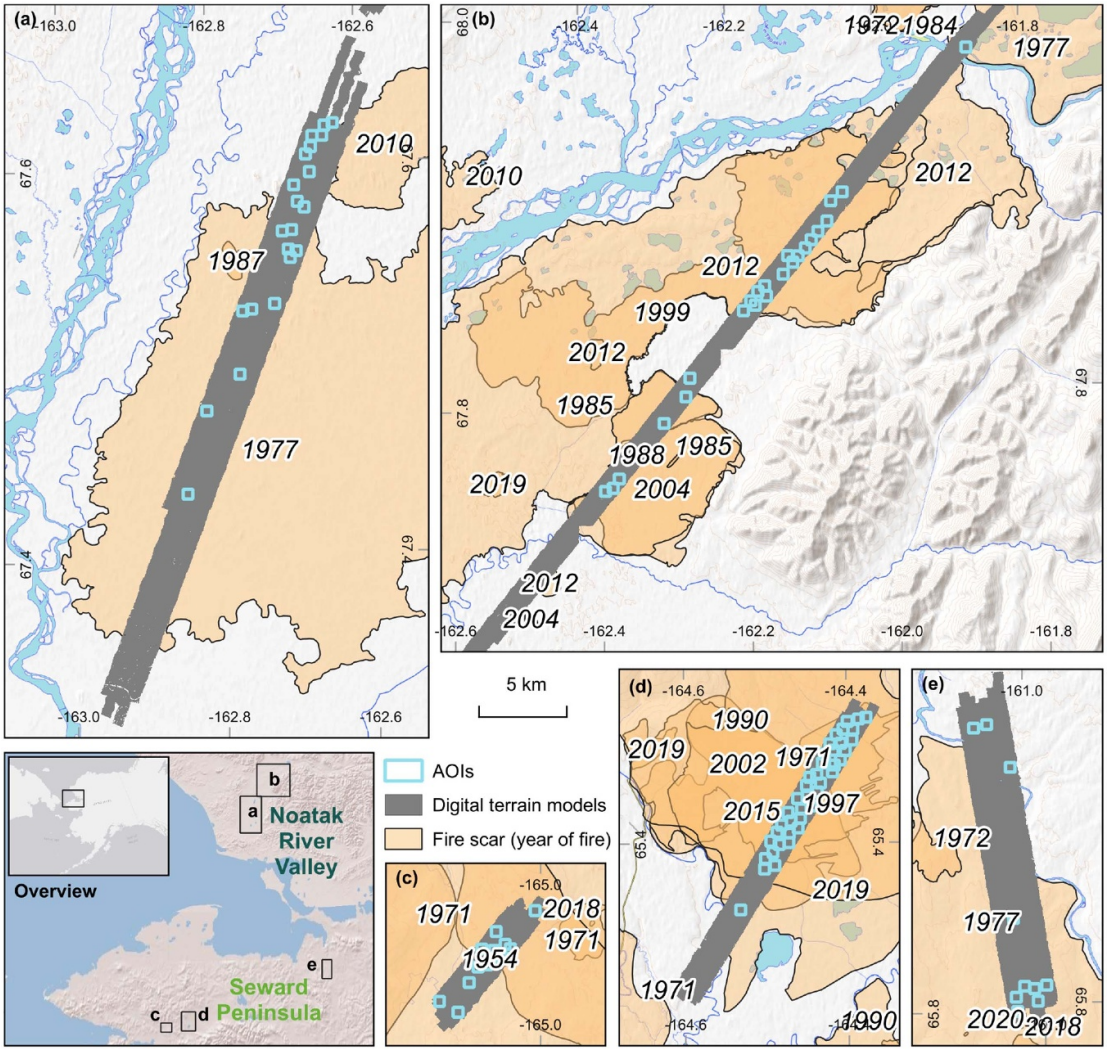

Figure 1. Location of the 106 studied AOIs within West Alaska. 44 are located in the Noatak River Valley (NRV, subfigures (a) and (b)), and 62 are located on Seward Peninsula (SP, subfigures (c)–(e)). The maps also show the outlines of the fire scars, their year of burn, and overlapping swaths of airborne-lidar derived high-resolution terrain models. Darker color tones in the fire scars indicate multiple burns during the observation period. Maps displayed in Polar Stereographic projection; north up.

eolian and the AOIs are located within the Yedoma region [32, 33]; the remaining are characterized by fluvial or coastal deposits. In the NRV, our AOIs are mostly characterized by deposits with moderate ice content and a silty to rocky composition from fluvial or glacial deposits.

3. Materials and methods

3.1. Datasets

3.1.1. Alaskan fire database

The ALFD was established in 1990 and includes records of Alaskan fires dating back until 1950, including information on the year, the area, and the location of burns (www.frames.gov/catalog/10465). Perimeters of the burn areas were mapped with a variety of delineation methods, including ground surveys, airborne surveys, and manual and automated mapping from aerial photography or satellite imagery. Due to these at times unconstricted mapping approaches, fire perimeters may be over- or underestimated and uncertainties are usually higher in remote areas and for older fire perimeters [40]. The database also does not contain records on the burn severity of the mapped fires. We used this database (as of August 2021, no version number) to determine the locations of fire scars and place our study areas within their boundaries.

3.1.2. Elevation models from airborne lidar

We use point clouds from airborne lidar to derive digital terrain models (DTMs) at high spatial resolution and accuracy. The lidar data was collected during an airborne survey campaign in Western Alaska between 25 June and 10 July 2021 with a full-waveform Riegl LMS-Q680i sensor. With a flight

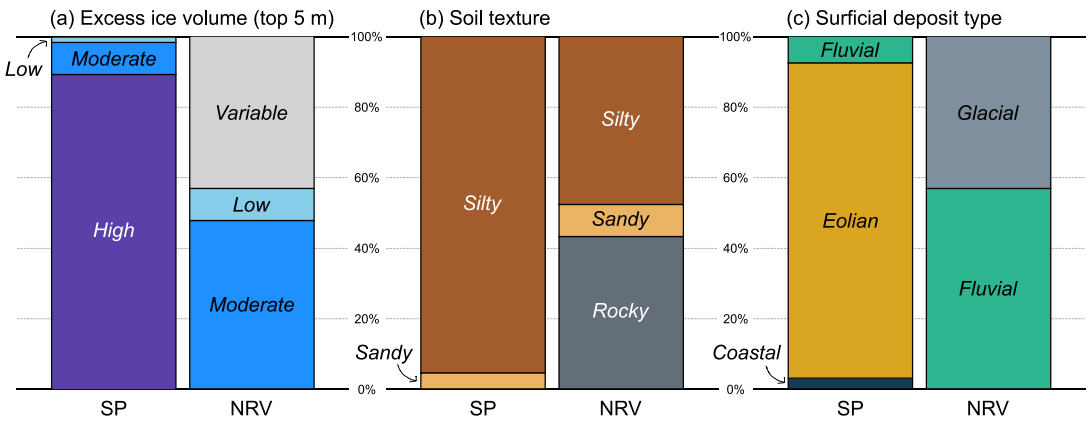

Figure 2. Overall distribution of ground ice and deposit characteristics for the AOIs in the two study regions SP and NRV. Data based on [31].

altitude of ca. 500 m AGL (above ground level), the point cloud density reached on average 5 pts m^{-2}. To generate elevation models from these point clouds, we conducted the following three steps:

(i) We used the echo width, the amplitude, and the target counter to classify the multiple target waveforms into the two classes of vegetation and of bare ground.
(ii) We used the global navigation satellite system-corrected flight trajectories (through precise point positioning processing), the inertial navigation system data, and information on squint angle and lever arms to correct and reference the point cloud's ground returns to WGS84.
(iii) Finally, we used inverse distance weighting to interpolate between points and generate a DTM.

The resulting DTM has a ground sampling distance of 1 m, with a vertical accuracy of 0.10 m.

3.2. Space-for-time substitution analysis

As we aim to investigate the evolution of polygonal ground within fire scars over time, a time-series analysis would be the obvious method for investigation. However, long-term temporal observations of a single study area do not exist and thus unfortunately render such an endeavor impossible. We have therefore opted for a space-for-time substitution approach, where we use spatial variation as a proxy for temporal change [41, 42]. With this approach we assume that any other environmental factors do not have significant influence on the degradation process; or alternatively, have equal influence throughout the analyzed study areas. Our 106 AOIs are located within and next to fire scars of varying ages, capturing the landscape under varying levels of degradation or stabilization and pre-burn/unburned states, respectively, and thus the approach takes some environmental variability into account. With the exception of one fire scar, we have multiple AOIs in each scar, which helps account for differences within a site. To account for potential variability in environmental conditions, we evaluate the more northerly NRV and the more southerly SP separately. Figures 1(a)–(e) provide an overview of our study sites.

3.3. Image-to-graph transformation

Within the 106 AOIs, we analyzed the microtopography of the landscape. In order to quantify and compare the polygonal terrain accurately, we extracted a graph of the network from the terrain models of each AOI. For this, we applied the method introduced by [20] which follows these four steps:

(i) Detrend the DTM to remove the regional topographic trend.
(ii) Binarize and denoise the image to generate a raster with trough-pixels as foreground class and all other pixels as background class.
(iii) Skeletonize the binary image to keep only the centerline of the troughs.
(iv) Convert the skeleton to a graph using the `networkx` python package.

The resulting graph is directed, with edges being defined by an ordered pair of nodes u and v. The direction of the edge is defined by the direction of hydrological flow and leads from the higher-elevated node u to the lower-lying node v. We extract the information on the respective nodes' elevation from the original DTM. Figure 3 shows three exemplary graphs from (a) unburned terrain, (b) terrain in a recent fire scar, and (c) terrain in an old fire scar.

3.4. Graph parameter extraction

To gather more information on the environmental properties of the trough network, we extracted information on its topological characteristics, as well

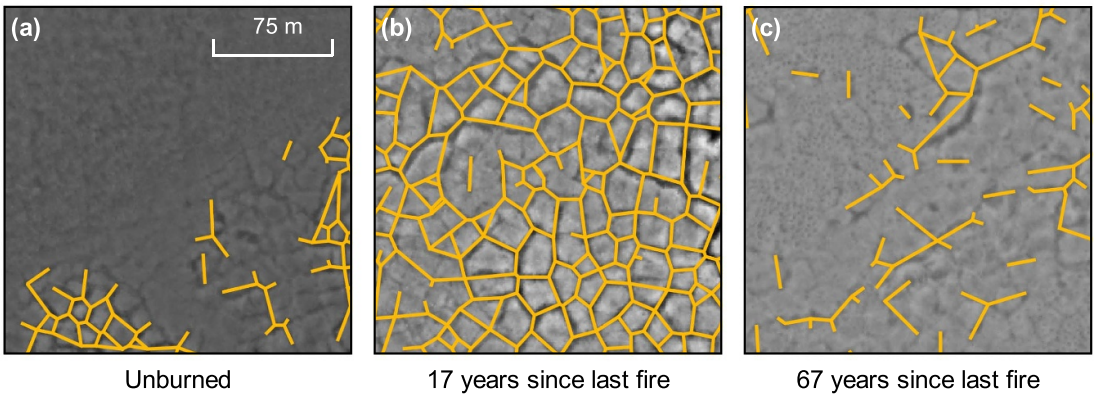

Figure 3. Graphs representing the polygonal network within three exemplary AOI subsets. The background shows the micro-topography (with regional trend removed). (a) Unburned reference area in the NRV region, (b) area burned in 1988 and 2004, also in the NRV region, and (c) area burned in 1954 in the SP region. The edges do not follow the exact paths of troughs in the visualization, but their true trajectories are captured within the edges' weights.

as on the presence of surface water within the troughs. Computed parameters (such as the length of a trough) are stored as weights of the respective edge. More details to this procedure are described in [20]. Compared to their approach, we have slightly adapted the methodology of extracting the surface water presence within troughs: When analyzing the trough transects, we checked if any two neighboring pixels have the exact same elevation (flat water surface) and if this elevation was below the mean elevation of the transect, we considered this part of the trough as water-filled. We then collected the number of pixels within a trough that are water-filled and also saved this information towards the edge weights. If all pixels within a trough were water-filled, this number would amount to 1, and we assumed that water was potentially flowing between the two trough intersections at the beginning and end of this trough.

3.5. Quantitative network analysis

Once the graphs were extracted from the DTMs and all necessary information on the trough topographies and environment was stored within the nodes and edges, we conducted the quantitative analysis for all study sites. In order to gather insights on the state of the polygonal trough network, we used metrics from graph theory: We looked at the number of graph edges (corresponding to the number of troughs), the number of connected components (corresponding to the number of hydrologically isolated networks), and the total channel length (in real-world distances, i.e. kilometers). To gather information on the actual hydrological state of these networks at the time of data acquisition, we also analyzed the percentage of water-filled troughs per AOI.

For the pseudo-temporal evolution of these four network parameters post-disturbance, we fitted a second-order regression between the youngest and the oldest fire scars and report the R^2-value.

4. Results

Independent of an AOI being in the fire scar or in unburned ground, we observe a wide spread of values inter-class. This is an important foundation we need to keep in mind throughout the remaining analysis of results. We report all numbers as median ± MAD (median absolute deviation).

4.1. Seward Peninsula

In the SP study sites, we observe a large spread of trough numbers and lengths in the unburned reference ground (529 ± 463 troughs, 7.55 ± 6.08 km). Following the burn in year 0 (of the pseudo-time series), these numbers then increase to 2087 ± 203.5 troughs and 24.68 ± 1.99 km in the burnt terrain six years post-disturbance. After this rapid increase, the number of detected troughs and their total lengths decreased slowly but constantly until the conditions 67 years post-disturbance have almost recovered to numbers resembling the pre-burn state again (572 ± 185 troughs, 9.10 ± 2.70 km; figures 4(a) and (b)). With R^2 values of 0.256 and 0.275 respectively, the quadratic regression describes a moderate relationship between the fire age and the two metrics.

To gain further insights on the consequences of the networks' developments for the surface hydrology, we focused on the number of hydrologically isolated networks (number of connected components in graph-theory terms) and the percentage of inundated troughs per AOI (figures 4(c) and (d)). In the SP region, we observe an initial decrease for both metrics between pre-disturbance conditions and the first measurements after the burn (pre-burn: 36 ± 5 subnetworks, 33.0 ± 6.0% inundated; 6 year post-burn: 25 ± 8 subnetworks, 20.5 ± 3.5% of troughs inundated). This is then followed by an initially slow increase for both metrics, finally reaching values twice

as high as pre-burn conditions for the number of isolated subnetwork (67 year post-burn: 78 ± 14 subnetworks), and similar to pre-burn conditions for the water presence ($33.0 \pm 0.5\%$ of troughs are inundated). The R^2 values of the quadratic regression are reported as 0.432 for the number of subnetworks, and as 0.412 for the percentage of inundated troughs, hinting at a stronger relationship between fire scar age and recovery.

4.2. Noatak River Valley

In the NRV region, the unburned terrain already shows more elaborate polygonal networks than the terrain in SP does (albeit with a higher variability as well), with 1394 ± 997 troughs and 17.56 ± 9.61 km total channel lengths. Following the burn, we then generally observe similar trends for the analyzed topographical metrics as in SP: an initial increase in the first nine years (up to 1972.5 ± 762.5 troughs, 17.56 ± 9.61 km), followed by a subsequent decrease until the end of the analyzed pseudo-time series at 44 years post-burn (1106.5 ± 917.5 troughs, 14.60 ± 10.54 km; figures 4(e) and (f)). However, with only 33 AOIs spread over fire scars of only four different ages to fit the regression to, R^2 values drop to 0.159 and 0.192 for the number of troughs and the total channel length, respectively.

Concerning the network's hydrological characteristics, we observe a slight decrease in the number of subnetworks between the pre-burn conditions (46 ± 32 subnetworks) and the first observations post-burn (9 year post-burn: 32.5 ± 27.5 subnetworks, figure 4(g). This phase is followed by strongly decreasing numbers until the 17 year mark (9 ± 4 subnetworks), which again is followed by significantly higher numbers 22 and 44 years post-fire (69 ± 30 subnetworks and 36.5 ± 22.5 subnetworks, respectively). However, the R^2 of the quadratic regression is reported as 0.023, indicating a very low explained variation.

Looking at the percentage of inundated troughs (figure 4(h)), we observe $28.0 \pm 12.0\%$ of troughs being inundated in unburned terrain. Terrain nine years post-fire reports similar numbers, albeit with considerably lower intra-class variability with $33.0 \pm 2.5\%$ of troughs being inundated. We see a further increase until 17 years post-fire ($50.0 \pm 4.0\%$), followed by decreasing inundation until the end of our observations (44 year post-burn: $29.0 \pm 4.0\%$ of troughs inundated). This trend is opposite to the observations in SP, albeit the R^2 being a little lower at 0.324.

5. Discussion

Our analysis shows that polygonal permafrost terrains can follow variable pathways of degradation after experiencing disturbances such as tundra fires. Across both study regions, we observe that areas that have burned recently (up to two decades ago) generally show more elaborate trough networks than unburned areas. Translating this into the pseudo-time domain, this implies a rapid degradation of the polygonal landscape in the first years following a burn, which is in line with existing local field studies of post-fire recovery [17, 43]. When looking at older fire scars, we observe wide ranges of surface degradation: Some AOIs in older scars exhibit values comparable to AOIs in unburned terrain, while other individual AOIs remain highly degraded. On average, we do however observe some degree of stabilization and recovery: For the SP study site, the median number of troughs in the AOIs that have burned 67 years ago are almost as low as in the unburned reference AOIs; more than 25% of the variance can be explained by time alone.

In the NRV region, the unburned AOIs, as well as those in older fire scars, also show a stronger spread of values than in the AOIs from more recent fires. For NRV, the oldest sampled scars date to only 44 years though, and thus match the age of the AOIs in SP with the strongest spreads. Unfortunately, we do not have high-resolution DTMs covering older scars in NRV and therefore cannot assess if the trajectories would converge towards a smoothing after 60+ years post-disturbance. For all analyzed metrics, we report lower coefficients of determination than in the SP sites. Especially with the R^2 of 0.023 for regressing fire-scar age on the number of isolated troughs in NRV (figure 4(g)), we cannot derive a meaningful relationship between this variable and the age of a fire scar. Interestingly, in SP, this is the metric with the highest explained variation from the quadratic regression ($R^2 = 0.432$).

For the percentage of water-filled troughs, we observe contrasting regional trends with moderate to good explanatory power ($R^2 = 0.412$ in SP, $R^2 = 0.324$ in NRV). For SP, we see a rapid decrease, followed by a slow increase until the end of observations (figure 4(d)). This pattern follows models and observations made by e.g. [5, 44], where landscapes with higher network connectivity facilitate surface-water drainage. Assuming a slow infilling of troughs over time, the number of isolated subnetworks decreases (as observed in SP, figure 4(c)), reducing drainage pathways and promoting water retention. However, this mechanism cannot explain the opposing trend in NRV, where inundation increases until >17 years post-fire, followed by less degradation until the end of observations at 44 years post-fire. This trajectory also diverges from the other network metrics in the same region (figures 4(e)–(g)). These contrasting regional responses, combined with the substantial within-class variability (for all metrics), suggest that fire age alone

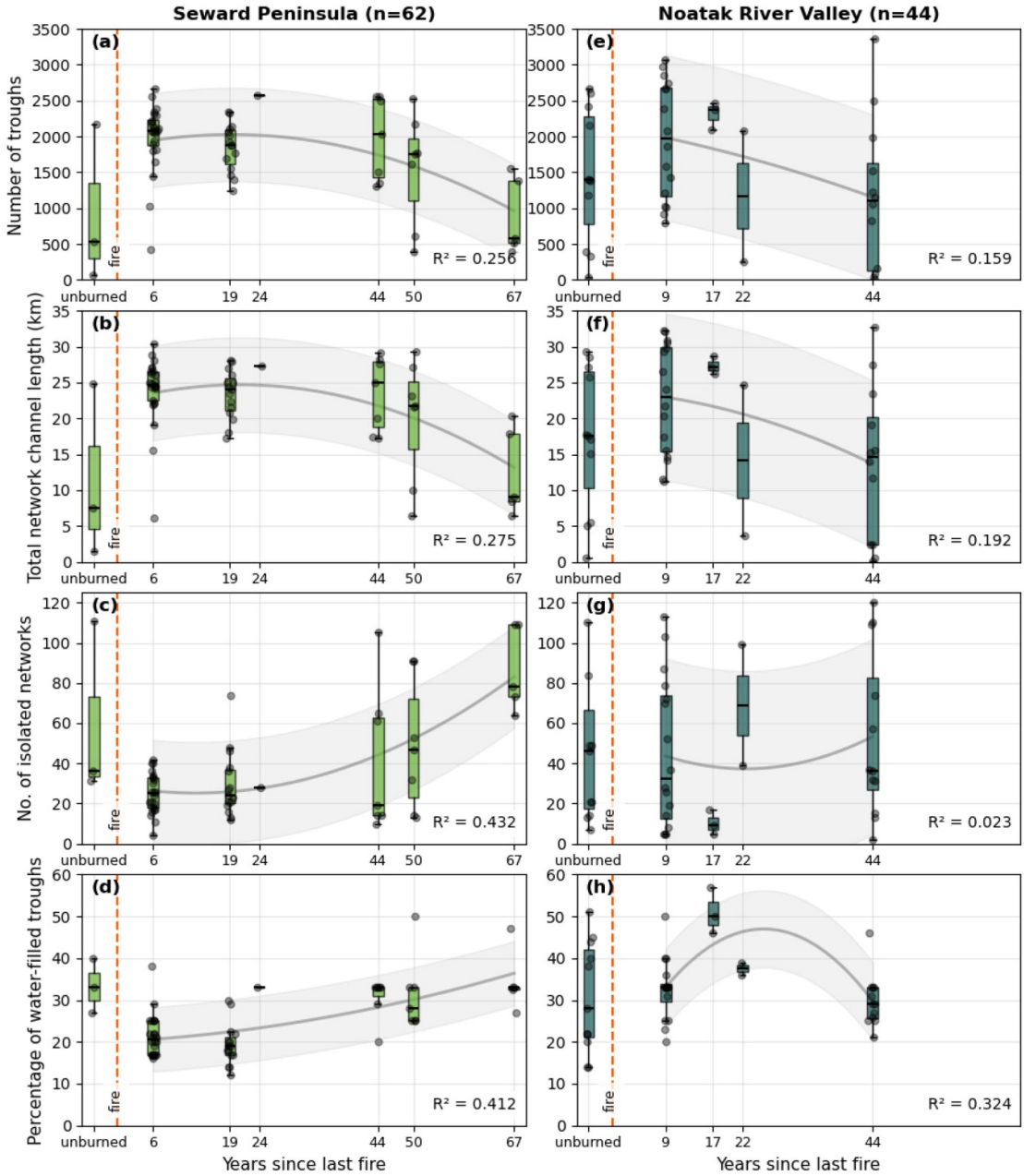

Figure 4. Pseudo-temporal evolution of post-fire morphological and hydrological characteristics in the polygonal terrain of the two study regions. Each point represents the value for an entire AOI. The gray curve denotes the quadratic fit, with the 95% confidence interval as bands.

cannot fully explain post-fire landscape evolution patterns.

So what drivers do influence the different pathways of landscape evolution and the high variability within individual fire scars? Previous studies support the narrative that the drainage conditions of soils and burn severity of fires can have a significant impact on the post-disturbance trajectories: In poorly drained landscapes, disturbed permafrost ground can recover faster, as wetter conditions promote easier peat accumulation in troughs and vegetation regrowth, effectively filling in the troughs and smoothing the landscape once again [15]. An alternative explanation may be that in poorly-drained soils the fires burned less severe to begin with [27]. In these cases, less of the insulating organic layer gets removed through the fire and the thermal impact on the underlying permafrost is smaller [45]. In the NRV study area, we observe the AOIs of the oldest burns to show less elaborate trough networks (on average) than the unburned plots do. Here, the abundance of lakes in the southern NRV study area (figure 1(a)), the percentage of inundated troughs at these sites, and measurements by [27] support local drainage conditions as a potential

control. However, the absence of burn severity data, especially for many older scars, limits definitive attribution.

5.1. Detecting historical fires on the Alaskan North Slope

Our observations of a general trend towards landscape stabilization and recovery over longer time scales initially appear to be in contrast with some studies made on the Alaskan North Slope [24, 46]. In [24], two large and previously undocumented fire scars, the Meade River Fire and the Ketik River Fire, were visually identified from aerial overflights in 2011 and 2012. Through historical image analysis and radiocarbon dating of charcoal material, the authors could date the fires to pre-1940 CE, implying them to be more than 70 years old at the time of their investigation. From in-situ measurements, they reported significant landscape differences between burned ground and the neighboring unburned areas, with different vegetation patterns and higher terrain rugosity within the bounds of the fire scar. In our studied regions, however, some of the oldest fire scars exhibited fewer troughs than younger burns, almost resembling unburned terrain characteristics. Especially comparing to the SP, which is, similar to the North Slope, also a Yedoma-rich terrain [32], we would expect more similar observations. One possible explanation for this discrepancy might lie in the trajectory variability: the Meade River Fire and the Ketik River Fire may represent the slowest-recovering endmembers of a broader spectrum of responses (i.e. the border cases, where trough networks remain visually recognizable for longer periods). This interpretation highlights an important detectability bias: Historical fire scars that have followed a more rapid trajectory of landscape stabilization and surface smoothing are less likely to be identified from aerial view or imagery. Even though we observe a slight recovery trend throughout our analysis, the large spread of landscape states after 40+ years suggests that various outcomes are possible: degraded polygonal landscapes may persist for many decades, or the trough network may recover to a state indistinguishable[11] from unburned terrain within the same time window. As a result, general conclusions drawn solely from visually detectable historical fire scars may be subject to survivorship bias.

5.2. The effect of climate warming

Considering the general trend of warming ground temperatures and a decline in permafrost extent induced by global warming, the slower pathways of recovery (regardless of disturbance) are not necessarily surprising and in line with observations described by [47]. Burned permafrost terrain is particularly sensitive to additional warming [15]; therefore, pathways of longer stabilization times observed are consistent with accelerating regional climate change. It is therefore also important to note that future recovery trajectories may not necessarily resemble the patterns inferred here, and that stabilization after disturbance may become increasingly delayed.

5.3. Limitations from datasets and methods

It is important to keep in mind that our space-for-time substitution still only provides an approximation of post-fire recovery rather than a true reconstruction of temporal change. Although we selected study sites with comparable soil and environmental conditions (section 2), it cannot be guaranteed that differences observed between unburned areas and older burn scars are purely age-related. Spatial heterogeneity can still also influence recovery trajectories, as factors such as local topography [47], snow distribution, surface characteristics [15, 48], or burn severity [49, 50][12] can impact the rate of recovery post-disturbance.

Further, the graph-based methodology of trough detection is only robust in high-centered polygonal terrain [20], and as such, we can only investigate post-fire landscape evolution in areas characterized by ice-wedge trough networks in the first place. Our analysis does not cover post-disturbance pathways in other permafrost landscapes.

Finally, it is necessary to acknowledge that the ALFD may contain errors in terms of exact fire perimeters. Older fire scars were delineated more coarsely based on lower-resolution imagery, or even just through rough estimates in the field. Unburned islands within a fire scar are also not necessarily always captured in the database [40]. The ALFD does not extend beyond 1950 and the authors further do not guarantee the fire record since then to be complete. These uncertainties introduce the possibility that some AOIs were misclassified; for example, placed in areas mapped as burned that may not have experienced fire, vice-versa, or unknowingly sampled within unrecorded unburned inclusions. Similarly, AOIs positioned near mapped perimeter boundaries could be affected by delineation errors. While there is no straightforward way to fully account for such issues without extensive manual validation using historical imagery, our sampling strategy of selecting multiple AOIs per fire scar helps reduce the adverse effects of delineation biases.

[11] Indistinguishable in DTMs.

[12] According to [51] burn severity is only a significant factor in glacial deposits, though.

6. Conclusion

In this study, we applied a space-for-time substitution based on high-resolution airborne lidar to quantify the states of trough networks in polygonal permafrost landscapes across a chronosequence of fire scars in Western Alaska. Our results demonstrate that tundra fires can substantially influence trough expression in the years immediately following disturbance. With increasing time since a burn, we observe a general trend towards a reduced microtopographic relief, which hints at partial stabilization and surface smoothing on decadal time scales.

However, this trajectory is not uniform. The substantial spread of values within scars of similar age suggests that post-fire evolution can proceed along multiple pathways. Some older scars exhibit trough networks that are less distinguishable from unburned terrain, others retain pronounced trough networks. This variability shows that fire age alone is not sufficient to predict the evolution of polygonal networks post-disturbance, but that additional factors, e.g. vertical drainage, substrate conditions, or burn severity, need to be considered for a full understanding of the landscape response.

These varying pathways also have implications on how we understand and detect past fire activity. Scars that recover more rapidly may become topographically indistinct after several decades and thus remain unrecognized in remote sensing datasets. As a result, the long-term effects of tundra fires on the landscape may be underestimated, especially for fire scars predating the satellite record.

Despite this variability, our lidar-based framework provides a robust, scalable means to derive microtopographic metrics across large spatial extents and enables reproducible assessment of fire impacts beyond the scale of prior field studies. With the increasing availability of high-resolution airborne lidar data, the approach introduced in this study provides an important foundation for expanding fire scar analyses across both space and time, and with this, hopefully being able to deliver more robust insights, given the large inter-year variability in both fire scars and unburned ground. To ensure that such scaling is computationally feasible, we implemented our pipeline with Nextflow [52], a workflow manager that improves reproducibility, portability, and computational efficiency (see supplementary material B for details). By parallelizing across multiple CPUs, we achieved substantial speed-ups, demonstrating that even larger cluster deployments are technically viable. This capacity to process greater volumes of data opens the possibility of expanding future analyses to include broader climatic, environmental, geomorphologic and geologic gradients, to investigate larger number of fire histories, and to conduct repeated temporal observations in the same area. Such efforts will be substantial for investigating the drivers behind divergent recovery trajectories and for improving projections of permafrost landscape evolution under a rapidly changing fire regime in the Arctic.

Acknowledgments

T Rettelbach and B R Groenke acknowledge the support and funding through the Helmholtz Einstein International Berlin Research School in Data Sciences (HEIBRiDS). J Bader was funded by the Deutsche Forschungsgemeinschaft (DFG, German Research Foundation)—Project-ID 414984028—SFB 1404 FONDA. Additional support was provided by AWI by facilitating the Perma-X 2021 airborne campaign with the Polar-6 plane to acquire high-resolution lidar elevation data in Western Alaska. We thank the anonymous reviewers, as well as Anna Liljedahl and Wenwen Li for a friendly review and suggestions that helped to improve the study.

Data availability statement

The data that support the findings of this study are openly available at the following URL/DOI: https://doi.org/10.5281/zenodo.17866631, https://doi.org/10.5281/zenodo.18594026 [53, 54].

Author contributions

T Rettelbach 0000-0002-4187-4113
Conceptualization (equal), Data curation (supporting), Formal analysis (lead), Methodology (lead), Project administration (lead), Software (supporting), Validation (equal), Visualization (lead), Writing – original draft (lead), Writing – review & editing (lead)

J Bader 0000-0003-0391-728X
Conceptualization (supporting), Formal analysis (supporting), Methodology (supporting), Software (lead), Writing – original draft (supporting), Writing – review & editing (supporting)

B Groenke 0000-0003-2570-9342
Conceptualization (supporting), Formal analysis (supporting), Methodology (equal), Software (supporting), Validation (equal), Writing – original draft (supporting), Writing – review & editing (supporting)

V Helm 0000-0001-7788-9328
Data curation (lead), Investigation (supporting), Methodology (equal), Resources (equal), Software (supporting), Writing – original draft (supporting)

M Langer 0000-0002-2704-3655
Conceptualization (equal), Formal analysis (equal), Funding acquisition (supporting), Investigation (supporting), Methodology (supporting), Project administration (supporting), Supervision (equal), Writing – original draft (supporting)

J-C Freytag 0000-0002-5089-6875
Conceptualization (supporting), Funding acquisition (equal), Methodology (supporting), Resources (supporting), Supervision (equal), Writing – original draft (supporting)

G Grosse 0000-0001-5895-2141
Conceptualization (supporting), Funding acquisition (equal), Methodology (supporting), Project administration (supporting), Resources (equal), Supervision (equal), Writing – original draft (supporting)

References

[1] Biskaborn B K *et al* 2019 Permafrost is warming at a global scale *Nat. Commun.* **10** 264
[2] Miner K R, Turetsky M R, Malina E, Bartsch A, Tamminen J, McGuire A D, Fix A, Sweeney C, Elder C D and Miller C E 2022 Permafrost carbon emissions in a changing Arctic *Nat. Rev. Earth Environ.* **3** 55–67
[3] Schuur E A G *et al* 2015 Climate change and the permafrost carbon feedback *Nature* **520** 171–9
[4] Ogden E L, Cumming S G, Smith S L, Turetsky M R and Baltzer J L 2023 Permafrost thaw induces short-term increase in vegetation productivity in northwestern Canada *Glob. Change Biol.* **29** 5352–66
[5] Liljedahl A K *et al* 2016 Pan-Arctic ice-wedge degradation in warming permafrost and its influence on tundra hydrology *Nat. Geosci.* **9** 312–8
[6] Webb H *et al* 2025 A review of abrupt permafrost thaw: definitions, usage and a proposed conceptual framework *Curr. Clim. Change Rep.* **11** 1–15
[7] Jones B M, Grosse G, Arp C D, Miller E, Liu L, Hayes D J and Larsen C F 2015 Recent Arctic tundra fire initiates widespread thermokarst development *Sci. Rep.* **5** 15865
[8] Liljedahl A, Hinzman L, Busey R and Yoshikawa K 2007 Physical short-term changes after a tussock tundra fire, Seward Peninsula, Alaska *J. Geophys. Res.: Earth Surf.* **112** F02S07
[9] Chen Y, Lara M J and Hu F S 2020 A robust visible near-infrared index for fire severity mapping in Arctic tundra ecosystems *ISPRS J. Photogramm. Remote Sens.* **159** 101–13
[10] Young A M, Higuera P E, Duffy P A and Hu F S 2017 Climatic thresholds shape northern high-latitude fire regimes and imply vulnerability to future climate change *Ecography* **40** 606–17
[11] Mack M C, Bret-Harte M S, Hollingsworth T N, Jandt R R, Schuur E A G, Shaver G R and Verbyla D L 2011 Carbon loss from an unprecedented Arctic tundra wildfire *Nature* **475** 489–92
[12] Mackay J R 1995 Active layer changes (1968 to 1993) following the forest-tundra fire near Inuvik, NWT, Canada *Arct. Alp. Res.* **27** 323–36
[13] Keuper F, Dorrepaal E, van Bodegom P M, van Logtestijn R, Venhuizen G, van Hal J and Aerts R 2017 Experimentally increased nutrient availability at the permafrost thaw front selectively enhances biomass production of deep-rooting subarctic peatland species *Glob. Change Biol.* **23** 4257–66
[14] Frost G V, Loehman R A, Saperstein L B, Macander M J, Nelson P R, Paradis D P and Natali S M 2020 Multi-decadal patterns of vegetation succession after tundra fire on the Yukon-Kuskokwim Delta, Alaska *Environ. Res. Lett.* **15** 025003
[15] Holloway J E, Lewkowicz A G, Douglas T A, Li X, Turetsky M R, Baltzer J L and Jin H 2020 Impact of wildfire on permafrost landscapes: a review of recent advances and future prospects *Permafr. Periglac. Process.* **31** 371–82
[16] Rocha A V, Loranty M M, Higuera P E, Mack M C, Hu F S, Jones B M, Breen A L, Rastetter E B, Goetz S J and Shaver G R 2012 The footprint of Alaskan tundra fires during the past half-century: implications for surface properties and radiative forcing *Environ. Res. Lett.* **7** 044039
[17] Jones B M, Kolden C A, Jandt R, Abatzoglou J T, Urban F and Arp C D 2009 Fire behavior, weather and burn severity of the 2007 Anaktuvuk River tundra fire, North Slope, Alaska *Arct. Antarct. Alp. Res.* **41** 309–16
[18] Liu L, Jafarov E E, Schaefer K M, Jones B M, Zebker H A, Williams C A, Rogan J and Zhang T 2014 InSAR detects increase in surface subsidence caused by an Arctic tundra fire *Geophys. Res. Lett.* **41** 3906–13
[19] Iwahana G, Uchida M, Liu L, Gong W, Meyer F J, Guritz R, Yamanokuchi T and Hinzman L 2016 InSAR detection and field evidence for thermokarst after a tundra wildfire, using ALOS-PALSAR *Remote Sens.* **8** 218
[20] Rettelbach T, Langer M, Nitze I, Jones B, Helm V, Freytag J-C and Grosse G 2021 A quantitative graph-based approach to monitoring ice-wedge trough dynamics in polygonal permafrost landscapes *Remote Sens.* **13** 3098
[21] Jones B M, Kanevskiy M Z, Shur Y, Gaglioti B V, Jorgenson M T, Jones M K W, Veremeeva A, Miller E A and Jandt R 2024 Post-fire stabilization of thaw-affected permafrost terrain in northern Alaska *Sci. Rep.* **14** 8499
[22] Kanevskiy M, Shur Y, Jorgenson T, Brown D R N, Moskalenko N, Brown J, Walker D A, Raynolds M K and Buchhorn M 2017 Degradation and stabilization of ice wedges: implications for assessing risk of thermokarst in northern Alaska *Geomorphology* **297** 20–42
[23] Kanevskiy M *et al* 2022 The shifting mosaic of ice-wedge degradation and stabilization in response to infrastructure and climate change, Prudhoe Bay Oilfield, Alaska, USA *Arct. Sci.* **8** 498–530
[24] Jones B M, Breen A L, Gaglioti B V, Mann D H, Rocha A V, Grosse G, Arp C D, Kunz M L and Walker D A 2013 Identification of unrecognized tundra fire events on the north slope of Alaska *J. Geophys. Res.: Biogeosci.* **118** 1334–44
[25] Narita K, Harada K, Saito K, Sawada Y, Fukuda M and Tsuyuzaki S 2015 Vegetation and permafrost thaw depth 10 years after a tundra fire in 2002, Seward Peninsula, Alaska *Arct. Antarct. Alp. Res.* **47** 547–59
[26] Barrett K, Rocha A V, van de Weg M J and Shaver G 2012 Vegetation shifts observed in Arctic tundra 17 years after fire *Remote Sens. Lett.* **3** 729–36
[27] He J, Chen D, Jenkins L and Loboda T V 2021 Impacts of wildfire and landscape factors on organic soil properties in Arctic tussock tundra *Environ. Res. Lett.* **16** 085004
[28] Obu J, Westermann S, Kääb A and Bartsch A 2018 *Ground Temperature Map: 2000–2016: Northern Hemisphere Permafrost* (Pangaea)
[29] Hollingsworth T N, Breen A L, Hewitt R E and Mack M C 2021 Does fire always accelerate shrub expansion in Arctic tundra? Examining a novel grass-dominated successional trajectory on the Seward Peninsula *Arct. Antarct. Alp. Res.* **53** 93–109
[30] French N H F, Jenkins L K, Loboda T V, Flannigan M, Jandt R, Bourgeau-Chavez L L and Whitley M 2015 Fire in

Arctic tundra of Alaska: past fire activity, future fire potential and significance for land management and ecology *Int. J. Wildland Fire* **24** 1045–61
[31] Jorgenson M T, Yoshikawa K, Kanevskiy M, Shur Y, Romanovsky V, Marchenko S, Grosse G, Brown J and Jones B 2008 Permafrost characteristics of Alaska *Proc. 9th Int. Conf. on Permafrost* vol 3 (University of Alaska Fairbanks) pp 121–2
[32] Strauss J *et al* 2021 Circum-Arctic map of the Yedoma permafrost domain *Front. Earth Sci.* **9** 758360
[33] Strauss J *et al* 2022 *Database of Ice-Rich Yedoma Permafrost Version 2 (IRYP v2)* (PANGAEA) (https://doi.org/10.1594/PANGAEA.940078)
[34] Raynolds M and Walker D 2022 *Raster Circumpolar Arctic Vegetation Map, V2* (Mendeley Data) (https://doi.org/10.17632/c4xj5rv6kv.2)
[35] Alaska Climate Research Center 2021 Annual report 2020 *Annual Report* (Alaska State Climate Center) 28 (available at: https://akclimate.org/data/annual-reports/?years = 2020)
[36] Yi Y and Kimball J S 2020 *ABoVE: Active Layer Thickness from Remote Sensing Permafrost Model, Alaska, 2001–2015* (ORNL DAAC) (https://doi.org/10.3334/ORNLDAAC/1760)
[37] Hugelius G *et al* 2013 A new data set for estimating organic carbon storage to 3 m depth in soils of the northern circumpolar permafrost region *Earth Syst. Sci. Data* **5** 393–402
[38] Reichle R, De Lannoy G, Koster R D, Crow W T, Kimball J S, Liu Q, and Bechtold M 2022 *MAP L4 Global 3-hourly 9 km EASE-Grid Surface and Root Zone Soil Moisture Geophysical Data, Version 7* (NASA National Snow and Ice Data Center Distributed Active Archive Center) (available at: https://nsidc.org/data/SPL4SMGP/versions/7)
[39] Hrobak J L and Schmunk G 2024 *Alaska Large Fire Database* (Bureau of Land Management) (available at: www.frames.gov/catalog/10465)
[40] Kasischke E S, Williams D and Barry D 2002 Analysis of the patterns of large fires in the boreal forest region of Alaska *Int. J. Wildland Fire* **11** 131–44
[41] Michaelides R J, Schaefer K, Zebker H A, Parsekian A, Liu L, Chen J, Natali S, Ludwig S and Schaefer S R 2019 Inference of the impact of wildfire on permafrost and active layer thickness in a discontinuous permafrost region using the remotely sensed active layer thickness (ReSALT) algorithm *Environ. Res. Lett.* **14** 035007
[42] Cao Z and Furuya M 2025 Decades-long evolution of post-fire permafrost deformation detected by InSAR: insights from chronosequence in North Yukon *AGU Adv.* **6** e2025AV001849
[43] Heim R J, Bucharova A, Brodt L, Kamp J, Rieker D, Soromotin A V, Yurtaev A and Hölzel N 2021 Post-fire vegetation succession in the Siberian subarctic tundra over 45 years *Sci. Total Environ.* **760** 143425
[44] Abolt C J *et al* 2024 Topography controls variability in circumpolar permafrost thaw pond expansion *J. Geophys. Res.: Earth Surf.* **129** e2024JF007675
[45] Jafarov E E, Romanovsky V E, Genet H, McGuire A D and Marchenko S S 2013 The effects of fire on the thermal stability of permafrost in lowland and upland black spruce forests of interior Alaska in a changing climate *Environ. Res. Lett.* **8** 035030
[46] Miller E A, Baughman C A, Jones B M and Jandt R R 2024 Biophysical effects of an old tundra fire in the brooks range foothills of Northern Alaska, USA *Polar Sci.* **39** 100984
[47] Smith S L, Riseborough D W and Bonnaventure P P 2015 Eighteen year record of forest fire effects on ground thermal regimes and permafrost in the Central Mackenzie Valley, NWT, Canada *Permafr. Periglac. Process.* **26** 289–303
[48] Farquharson L M, Mann D H, Grosse G, Jones B M and Romanovsky V E 2016 Spatial distribution of thermokarst terrain in Arctic Alaska *Geomorphology* **273** 116–33
[49] Brown R J E1983 Effects of fire on the permafrost ground thermal regime *The Role of Fire in Northern Circumpolar Ecosystems* ed R W Wein and D A MacLean (Wiley) pp 97–110
[50] Racine C H, Dennis J G and Patterson W A III 1985 Tundra fire regimes in the Noatak river watershed, Alaska: 1956–83 *Arctic* **38** 194–200
[51] Chen Y, Lara M J, Jones B M, Frost G V and Hu F S 2021 Thermokarst acceleration in Arctic tundra driven by climate change and fire disturbance *One Earth* **4** 1718–29
[52] Di Tommaso P, Chatzou M, Floden E W, Barja P P, Palumbo E and Notredame C 2017 Nextflow enables reproducible computational workflows *Nat. Biotechnol.* **35** 316–9
[53] Rettelbach T *et al* 2025 Supporting datasets for "Post-disturbance ice-wedge degradation in Alaskan tundra fire scars using space-for-time substitution remote sensing" *Zenodo* (https://doi.org/10.5281/zenodo.17866631)
[54] Rettelbach T and Bader J 2026 trettelbach/chrono-sequence_tundra_fires: Code to reproduce results for publication "Post-disturbance ice-wedge degradation in Alaskan tundra fire scars using space-for-time substitution remote sensing" (v1.0.1) *Zenodo* (https://doi.org/10.5281/zenodo.18594026)